Tetrahedron 67 (2011) 3317–3327

Contents lists available at ScienceDirect

Tetrahedron

journal homepage: www.elsevier.com/locate/tet

Synthesis and structural, spectroscopic, and electrochemical characterization of benzo[c]quinolizinium and its 5-aza-, 6-aza, and 5,6-diaza analogues

Aleksandra Jankowiak [a], Emilia Obijalska [a,b,†], Piotr Kaszynski [a,b,*], Adam Pieczonka [a,b,§], Victor G. Young, Jr. [c]

[a] Organic Materials Research Group, Department of Chemistry, Vanderbilt University, Box 1822 Station B, Nashville, TN 37235, USA
[b] Faculty of Chemistry, University of Łódź, Tamka 12, 91403 Łódź, Poland
[c] Crystallographic Laboratory, Department of Chemistry, University of Minnesota, Twin Cities, MN 55455, USA

ARTICLE INFO

Article history:
Received 4 December 2010
Received in revised form 4 March 2011
Accepted 9 March 2011
Available online 16 March 2011

ABSTRACT

Four heterocyclic salts **1a**–**d** were prepared by Ca^{2+}-assisted cyclization of fluoro derivatives **3**, and investigated by spectroscopic (NMR and UV), electrochemical, and computational (DFT and MP2) methods. The mechanism for the formation of the cations was investigated at the DFT level of theory. 2-D NMR spectroscopy for **1**[ClO_4] in DMSO-d_6 aided with DFT results permitted the assignment of ^1H and ^{13}C NMR signals in cations **1**. The molecular and crystal structures for **1a**[ClO_4] [$C_{13}H_{10}ClNO_4$ triclinic, $P\bar{1}$, a=9.6517(12) Å, b=11.0470(13) Å, c=12.2373(15) Å, α=67.615(1)°, β=78.845(2)°, γ=87.559(2)°; V=1183.0(2) Å^3, Z=4] and **1d**[ClO_4] [$C_{12}H_9ClN_2O_4$ triclinic, $P\bar{1}$, a=5.9525(6) Å, b=8.3141(9) Å, c=12.2591 (13) Å, α=73.487(1)°, β=83.814(1)°, γ=83.456(1)°; V=576.07(10) Å^3, Z=2] were determined by X-ray crystallography and compared with results of DFT and MP2 calculations. Electrochemical analysis gave the reduction potential order (**1b**>**1c**~**1d**>**1a**), which is consistent with computational results.

1. Introduction

The benzo[c]quinolizinium[1,2] (**1a**) and several of its derivatives[3,4] have been known for over four decades. The cation has been intensely investigated as a possible pharmacophore for the treatment of cystic fibrosis and diseases related to smooth muscle cell constriction, such as arterial hypertension and asthma.[5] It has also been used as a structural element of highly solvatochromic dyes[4] and columnar ionic liquid crystals.[6] Recently, a diaza analogue of **1a**, triazinium **1b**,[7,8] and an amino derivative of the mono-aza analogue **1c**[9] were described in the literature. It was demonstrated that **1b** is highly cytotoxic to cisplatin-resistant tumor cell lines,[7] intercalates to the minor groove of DNA,[8] and undergoes a reversible $1e^-$ reduction process.[8] For these reasons cations, such as **1a** and **1b** are attractive for development of pharmacologically active compounds and molecular materials with multi-redox properties, tunable electronic absorption spectra, and self-organization. Therefore, we focused on a series of cations **1a**–**d**, in which the CH groups in the bridging 5,6 positions of **1a** are systematically replaced with nitrogen atoms, and investigated the effect of the bridge modification on the molecular and electronic properties of the cations.

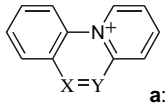

1

a: X = Y = CH
b: X = Y = N
c: X = N, Y = CH
d: X = CH, Y = N

The preparation of cation **1a** involves high temperature intramolecular cyclization of chlorostilbazole **2a** formally by intramolecular nucleophilic substitution reaction.[1] In contrast, the preparation of **1b** and **1c** involves 6π electrocyclization as the key step followed by oxidative rearomatization. Thus, the quinolizinium cation **1b** was obtained at ambient temperature in Au(III)-catalyzed light-induced electrocyclization of phenylazopyridine. Later, the Lewis acid was replaced with a Brønsted acid in preparation of **1b** and several of its derivatives.[8] The proposed mechanism involves sunlight trans-to-cis isomerization, acid-induced tautomerization, electrocyclization, and aerial oxidative rearomatization.[8] The reaction requires concentrated mineral acid and long exposures to light, which limits its practicality. The formation of 9-amino derivative of **1c** is a Cu(II)-mediated process in which

* Corresponding author. Tel.: +1 615 322 3458; e-mail address: piotr.kaszynski@vanderbilt.edu (P. Kaszynski).
† A visiting student from the laboratory of Professor Grzegorz Mloston, University of Łódź Poland.
§ In part described in M.Sc. Thesis, University of Łódź, Poland, 2008.

0040-4020/$ – see front matter © 2011 Elsevier Ltd. All rights reserved.
doi:10.1016/j.tet.2011.03.023

a radical cation formed by intramolecular one-electron transfer to the coordinated metal undergoes electrocyclization.[9] Cation **1c** was not formed under Brønsted acid conditions described for **1b**.[9]

We previously demonstrated that the azo group activates halogen toward nucleophilic aromatic substitution.[10] Particularly reactive was fluoride, which undergoes substitution with the thiolate at ambient temperature. Therefore, we considered fluorophenylazopyridine **3b** as a suitable substrate for a facile intramolecular cyclization to cation **1b** in which the fluoride is replaced by pyridine. Such a reaction could offer practical access to functionalized derivatives of **1b** under mild and pH neutral conditions, and could be extended to the preparation of remaining three cations **1a**, **1c**, and **1d**.

Here we describe the preparation of cations **1a**–**d** by Ca^{2+}-assisted intramolecular cyclization of fluorides **3**. The mechanism of this transformation is investigated with DFT computational methods. The effect of substitution of N for a CH in the cations on their molecular and electronic structures is probed using XRD, spectroscopic and electrochemical methods, and the experimental work is augmented with DFT and MP2 level calculations.

2. Results and discussion

2.1. Synthesis

Benzo[c]quinolizinium (**1a**) was prepared according to a modified literature procedure[1] by thermally induced cyclization of chloro derivative **2a** in benzonitrile at 160 °C in the presence of catalytic amounts of I_2, which permitted trans–cis equilibration. The product was obtained in 54% yield as the perchlorate salt **1a**[**ClO$_4$**] (Scheme 1).

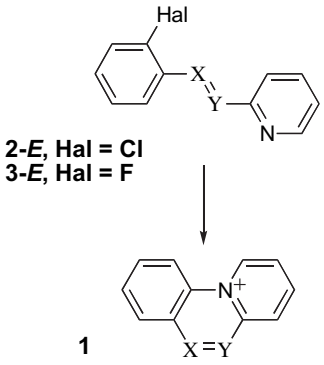

Scheme 1.

Similar thermal reaction of chloro diazene **2b** or fluoro diazene **3b** in benzonitrile in the absence of I_2, or in warm MeCN using sunlight or strong Pyrex-filtered halogen lamp light to effect trans–cis isomerization did not lead to the formation of the triazinium ion **1b**. No reaction of **2b** was observed either in refluxing MeCN nor in hot PhCN. Similar reactions of fluoro derivative **3b** were equally fruitless even though the fluoride usually is a significantly more mobile leaving group than chloride.

To activate the halogen toward displacement and intramolecular cyclization, we used an equimolar amount of AgOTs as a strong halophilic reagent. Reaction of chloro derivative **2b** conducted in warm MeCN irradiated with a halogen lamp led to the formation of **1b** in about 10% yield before the reaction was stopped by a silver mirror formed on the vessel's walls.

A reaction of the fluoro analog **3b** in warm MeCN in the presence of fluorophilic Ca^{2+} ions led to complete conversion of the substrate to the cation **1b**, isolated in ~80% yield as the tosylate **1b**[**OTs**]. The reaction mixture contained about 10% of water to ensure solubility of $Ca(OTs)_2$. No product formation was observed when the reaction was run without $Ca(OTs)_2$. Exposure of the reaction mixture to direct sunlight instead of halogen lamp was ineffective and no product formation was observed after several hours.

The Ca^{2+}-assisted cyclization proved to be successful also for the preparation of salts **1c** and **1d** from appropriate fluorides. Thus, thermal cyclization of **3c** and **3d** in hot PhCN in the presence of solid $Ca(OTs)_2$ gave complete conversion of the fluorides and formation of the cations as the main identifiable products. The reaction mixture contained substantial amounts of intractable products presumably formed by decomposition of the azomethine group labile under the reaction conditions. Cations **1c** and **1d** were isolated as perchlorates in 12% and 18% yield, respectively. The attempted cyclization of **3d** in (i) hot PhCN in the absence of $Ca(OTs)_2$, or (ii) in MeCN with $Ca(OTs)_2$ and irradiated with a halogen lamp gave only the starting material.

The auxiliary role of Ca^{2+} in the successful preparation of cations **1b**–**d** prompted us to investigate cyclization reactions of fluorostilbazole **3a** in the presence of $Ca(OTs)_2$. Under reaction conditions developed for the preparation of **1b** (MeCN, $Ca(OTs)_2$, halogen lamp, 10% water) fluoride **3a** showed the formation of cation **1a** as the sole product. The reaction time for the complete transformation of **3a** was longer that than for cyclization of **3b**, presumably due to lower absorption in the visible range of the spectrum. The same reaction of fluoride **3a** in the absence of $Ca(OTs)_2$ showed no product formation.

Preparation of stilbazoles **2a**[1] and **3a**[11] followed literature procedures and involved acetic anhydride-assisted condensation of appropriate halobenzaldehyde and 2-picoline (Scheme 2). Halodiazenes **2b** and **3b** were prepared by condensation of 2-chloronitrosobenzene[12] (**4**) and 2-fluoronitrosobenzene[13] (**5**), respectively, with 2-aminopyridine under basic conditions, as described for the chloro derivative **2b**.[12] Schiff bases **3c** and **3d** were prepared using standard acid-catalyzed condensation of appropriate aldehyde and amine (Scheme 2).

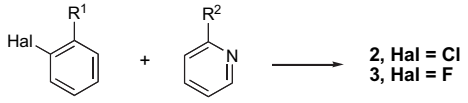

a: R^1 = CHO, R^2 = CH_3; Ac_2O
b: R^1 = NO, R^2 = NH_2; base
c: R^1 = NH_2, R^2 = CHO; acid cat.
d: R^1 = CHO, R^2 = NH_2; acid cat.

Scheme 2.

2.2. Molecular and crystal structures

Crystals of **1a**[**ClO$_4$**] and **1d**[**ClO$_4$**] were grown by slow evaporation of MeCN solutions. Solid-state structures for both compounds (Fig. 1) were determined by X-ray diffraction[14] and their selected bond lengths are shown in Table 1.

The two structures are essentially planar. The C(1)–N(11)–C(10a)–C(10) angle in cation **1a** is 2.1(2)° in molecule A and 5.6(2)° in molecule B. In the structure **1d**, the deviation from planarity is similar [2.4(3)°]. The cations are characterized by a short C(10a)–N(11) distance of 1.425(2) Å in both structures. This distance is comparable to that reported for 9-amino derivative of **1c** (1.424(3) Å),[9] longer than that observed in **1b** (1.401(5) Å),[8] and significantly shorter than the analogous Ph–N distance in *N*-phenylpyridinium[15] (1.45 Å). The short N–Ph distance is a consequence of the decreasing distance between the bridging atoms X(6)–Y(5) from 1.342(3) Å in **1a** through 1.297(3) Å in **1d** to the shortest, 1.275(6) Å in **1b**. With the falling X–Y distance, the C(1)···C(10) bay in the cations opens up by about 0.06 Å in **1b** in comparison to **1a** (Table 1). These results are well reproduced by computational methods (vide infra).

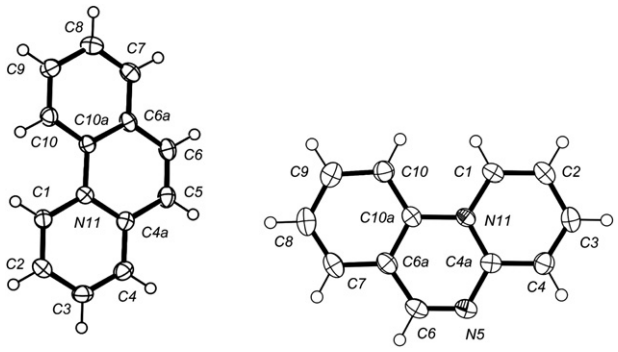

Fig. 1. Thermal ellipsoid diagram for **1a**[ClO_4] (molecule A) and **1d**[ClO_4] drawn at 50% probability. For clarity the anion is omitted. Interatomic distances are listed in Table 1. Atom numbering scheme according to the chemical structure.

Table 1
Selected experimental and calculated bond lengths for salts **1**[ClO_4]

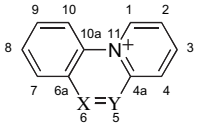

Distances/Å	1a		1b		1c	1d	
	Exptl[a]	Calcd[b]	Exptl[c]	Calcd[b]	Calcd[b]	Exptl[a]	Calcd
C(4)–C(4a)	1.402(2)	1.408	1.379(6)	1.400	1.400	1.397(3)	1.405
C(4a)–Y(5)	1.426(2)[d]	1.418[d]	1.387(5)[e]	1.376[e]	1.432[f]	1.372(2)[g]	1.354[g]
Y(5)–X(6)	1.342(3)[d]	1.353[d]	1.275(6)[e]	1.273[e]	1.290[f]	1.297(3)[g]	1.298[g]
X(6)–C(6a)	1.429(2)[d]	1.423[d]	1.387(5)[e]	1.377[e]	1.372[f]	1.422(3)[g]	1.425[g]
C(10a)–C(6a)	1.408(2)	1.415	1.401(5)	1.411	1.417	1.403(3)	1.410
C(10a)–N(11)	1.425(2)	1.426	1.401(5)	1.413	1.421	1.425(2)	1.422
C(1)–N(11)	1.379(2)	1.376	1.375(4)	1.369	1.370	1.376(2)	1.374
C(4a)–N(11)	1.384(2)	1.385	1.385(4)	1.377	1.378	1.384(2)	1.388
C(1)···C(10)	2.863	2.874	2.91	2.936	2.903	2.889	2.903

[a] Distances for molecule A. See Ref. 14.
[b] B3LYP/6-311G(2d,p) level geometry optimization at C_s point group symmetry. Numbering system according to the chemical structure.
[c] $CF_3SO_3^-$ salt, Ref. 8.
[d] X=Y=CH.
[e] X=Y=N.
[f] X=N, Y=CH.
[g] X=CH, Y=N.

The unit cell of **1a**[ClO_4] contains two distinct cations and two anions per asymmetric unit. These cations and anions are arranged about an approximate non-crystallographic local center at approximately (0.22, 0.73, 0.30). This serves only to increase the contents of the asymmetric unit to Z'=2. Both cations are disordered leading to exchange of the C(10a) and N(11) positions, each in different ratios: 0.95:0.05 in cation *A* and 0.72:0.28 in cation *B*. The cations are aligned approximately parallel to each other with the separation between them of about 3.35 Å.

In the unit cell of **1d**[ClO_4] there are two cations and two anions related by an inversion center. The cations form an infinite slipped stack allowing for partial overlap of the pyridinium rings separated by about 3.4 Å within the unit cell, and partial overlap of benzene rings between the unit cells separated by about 3.3 Å. Cations in the neighboring unit cells are nearly co-planar, and they are separated by C(4)···N(5) distance of 3.53 Å. Each pair is separated from the next by two anions.

2.3. Geometry optimization and selection of a computational model

For a better understanding of properties of cations **1**, we conducted quantum-mechanical calculations. To select a suitable computational protocol, equilibrium geometries of **1** were obtained with B3LYP and MP2(fc) methods and several bases sets, and results were compared to experimental solid-state structures of **1a**, **1b**, and **1d**.[16]

In general, all four cations converged to planar structures using the DFT method with four basis sets: 6-31G(d,p), 6-311G(2d,p), 6-311+G(2d,p), and cc-pVDZ, and the MP2 level of theory with 6-31G(d,p), 6-311G(2d,p), and cc-pVDZ basis sets. The only exception is cation **1a**, which is predicted by the MP2/6-31G(d,p) method to be twisted with the C(1)–N(11)–C(10a)–C(10) torsional angle of 6.7°.

Detailed comparison of theoretical and experimental bond lengths demonstrated that the DFT method performed better than the MP2 method in geometry optimization of cations **1**.[16] In both methods the cc-pVDZ basis set performed least satisfactory giving the largest mean error. Results closest to the experimental interatomic distances were obtained with the B3LYP/6-311G(2d,p) method, and selected data are shown in Table 1. For cations **1a** and **1d** the mean difference was 0.001±0.005 Å (absolute mean 0.004±0.005 Å), which is close to the typical experimental uncertainty of ±0.003 Å. The largest difference between the calculated and experimental distances was found for the C(5)–C(6) bond in **1a** and C(4a)–N(5) in **1d**. With these two results excluded from analysis the error decreases to 0.002±0.004 Å (absolute mean 0.003±0.002 Å). The same analysis for cation **1b** gave higher mean error 0.005±0.010 Å (absolute mean 0.010±0.005 Å) for all bonds, which is consistent with significant experimental uncertainty of ±0.006 Å (Table 1).

On the basis of geometry optimization results, the B3LYP/6-311G(2d,p) method was used in subsequent mechanistic studies (Table 2), assignment of NMR chemical shifts (Table 3), analysis of electronic absorption spectra (Table 4), and investigation of reduction for cations **1** (Table 5).

Table 2
Calculated relative free energy (kcal/mol) for compounds involved in conversion of chlorides **2** to **1** and fluorides **3** to **6** in MeCN[a]

		ΔG_{298} ***Z*—E**[b]	$\Delta G^{\ddagger}_{298}$[c] ***E*→*Z***	$\Delta G^{\ddagger}_{298}$[d] ***Z*→*E***	$\Delta G^{\ddagger}_{298}$ ***Z*-I→1-Cl** ***Z*-I→6**[e]	ΔG_{298} ***Z*-I–1-Cl** ***Z*-I–6**[e]
a	Cl	8.3	>45	>35	31.4	−23.7
	F	10.6	>45	>35	24.9	16.3
b	Cl	15.8	40.2	24.5	29.9	−17.8
	F	17.2	35.3	17.7	22.4	5.7
c	Cl	6.2	20.0	13.7	35.0	−15.5
	F	8.2	19.9	11.6	27.3	17.7
d	Cl	10.2	23.6	13.4	32.0	−20.6
	F	11.0	18.8	7.8	24.2	12.6

[a] B3LYP/6-311+G(2d,p)//B3LYP/6-311G(2d,p) level calculations in MeCN dielectric medium.
[b] $\Delta G_{298}=G_{298}(\boldsymbol{Z})-G_{298}(\boldsymbol{E})$ for the two global minima conformers ***Z*** and ***E***.
[c] $\Delta G^{\ddagger}_{298}$ for conversion of the global minimum conformer of ***E*** to ***Z***.
[d] $\Delta G^{\ddagger}_{298}$ for conversion of the global minimum conformer of ***Z*** to ***E***.
[e] Upper line $\Delta G_{298}=G_{298}(\boldsymbol{Z}\text{-}\mathbf{I})-G_{298}(\mathbf{1}\text{-}\mathbf{Cl})$. Cl^- coordinated to **1**. Lower line, $\Delta G_{298}=G_{298}(\boldsymbol{Z}\text{-}\mathbf{I})-G_{298}(\mathbf{6})$.

2.4. Mechanistic analysis

The mechanism for the formation of cations **1** from halo pyridine derivatives **2** and **3** involves ***E*** to ***Z*** isomerization and subsequent intramolecular attack of the pyridine N atom on the C(Hal) atom of the halophenyl ring. In principle, the cation **1** can be formed directly from the cis isomer or through non-aromatic cyclic product **6** (Scheme 3), which undergoes rearomatization upon departure of the halide. The success of the reaction depends on (i) the access to the *Z* isomer, and (ii) relative height of the barriers to cyclization versus back isomerization to the *E* isomer. To assess these factors, transformations of chloro and fluoro pyridine derivatives **2** and **3** to the cations **1** were investigated at the B3LYP/6-311+G(2d,p)//B3LYP/6-311G(2d,p) level of theory in MeCN dielectric medium without participation of metal ions.

Table 3
Assignment of experimental and calculated ^{13}C and ^{1}H NMR chemical shifts for **1**[ClO_4][a]

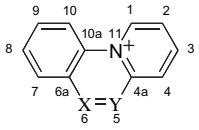

Nucleus	**1a**[b]		**1b**[c]		**1c**[d]		**1d**[e]	
	^{13}C	^{1}H	^{13}C	^{1}H	^{13}C	^{1}H	^{13}C	^{1}H
C(1)–H	134.6	10.40	133.0	10.51	134.9	10.54	134.1	10.31
	131.4	*9.80*	*129.9*	*9.77*	*131.6*	*9.91*	*130.7*	*9.68*
C(2)–H	124.3	8.29	129.2	8.74	128.7	8.64	124.5	8.36
	124.3	*8.02*	*130.5*	*8.45*	*129.6*	*8.36*	*125.1*	*8.05*
C(3)–H	140.6	8.65	146.0	9.18	143.7	8.99	145.2	8.83
	140.9	*8.40*	*147.0*	*9.00*	*144.2*	*8.76*	*145.0*	*8.64*
C(4)–H	128.5	8.70	130.5	9.46	129.1	9.01	131.4	8.68
	129.5	*8.37*	*133.4*	*9.27*	*130.6*	*8.67*	*131.2*	*8.54*
C(4a)	143.3	—	141.4	—	134.4	—	147.6	—
	143.7		*141.4*		*132.8*		*148.3*	
Y(5)	123.0	8.38	—	—	150.6	9.88	—	—
	123.1	*8.07*			*150.5*	*9.59*		
X(6)	136.6	8.74	—	—	—	—	162.4	10.00
	139.7	*8.54*					*164.0*	*9.66*
C(6a)	126.8	—	142.4	—	139.2	—	121.9	—
	127.7		*144.0*		*141.9*		*121.4*	
C(7)–H	130.5	8.40	132.3	9.13	131.2	8.44	130.8	8.63
	132.1	*8.30*	*136.4*	*9.18*	*134.1*	*8.55*	*132.9*	*8.47*
C(8)–H	130.5	8.08	133.3	8.42	132.4	8.18	131.5	8.23
	131.6	*8.05*	*134.9*	*8.45*	*133.9*	*8.21*	*133.0*	*8.20*
C(9)–H	132.9	8.21	138.9	8.60	132.5	8.22	137.6	8.49
	134.7	*8.23*	*142.8*	*8.59*	*135.3*	8.24	*140.4*	*8.48*
C(10)–H	118.1	9.16	116.8	9.23	117.7	9.15	117.3	9.17
	115.3	*8.83*	*114.0*	*8.76*	*115.0*	*8.80*	*115.0*	*8.80*
C(10a)	134.3	—	123.1	—	126.7	—	135.9	—
	135.5		*122.3*		*127.2*		*137.3*	

[a] Upper experimental data in DMSO-d_6, lower (italics) data derived from B3LYP/6-311+G(2d,p)//B3LYP/6-311G(2d,p) level calculations in DMSO dielectric medium. For details see Supplementary data.
[b] X=Y=CH.
[c] X=Y=N.
[d] X=N, Y=CH.
[e] X=CH, Y=N.

Table 4
Selected experimental[a] and calculated [b] electronic transition energies and oscillator strength for **1**[ClO_4]

Compound	Experimental[a]		Theoretical[b]
	Absorption λ_{max}/nm	Emission λ_{em} (λ_{ex})/nm	$\pi\rightarrow\pi^*$ (f)
1a[ClO_4]	363,[c] 257[d]	394 (347)[e]	341 (0.21), 281 (0.29), 259 (0.34)
1b[ClO_4]	359,[c] 259[f]	—[g]	340 (0.23), 268 (0.51)
1c[ClO_4]	363,[c] 242	394 (347)[e]	347 (0.18), 286 (0.13), 268 (0.34)
1d[ClO_4]	349,[c] 250	—	320 (0.15), 273 (0.19), 261 (0.45)

[a] Recorded in MeCN.
[b] Obtained with TD B3LYP/6-311+(2d,p)//B3LYP/6-311(2d,p) method in MeCN dielectric medium.
[c] The (0,0) transition.
[d] 365 nm (log ϵ=3.68) and 255 nm (log ϵ=4.07) in EtOH. Ref. 3.
[e] Excitation wavelength.
[f] Similar spectral characteristic reported in Ref. 8.
[g] Emission at 535 nm (λ_{ex}=340 nm) in MeCN reported in Ref. 8.

Initial computational effort concentrated on identifying global conformational minima for trans and cis isomers of **2** and **3** by comparison of SCF energies obtained in MeCN medium. Results for **2**-***E*** and **3**-***E*** showed that the most stable conformation for **a**, **b**, and **d** in MeCN is of type ***E*-IV**, while conformer ***E*-III** is the most stable form of **2c**-***E*** and **3c**-***E*** (Fig. 2). For the cis isomer the most stable conformers in MeCN are of type ***Z*-II** (**2c** and **3c**), ***Z*-III** (**2a**, **2b**, **3a**),

Table 5
Experimental and calculated electrochemical reduction potentials for **1**[ClO_4] versus SCE

Compound	Experimental[a]		Calculated[b]	
	$E_{1/2}^{1\ red}$ (+/•)/V	$E_{pc}^{1\ red}$[c] (+/•)/V	$E^{1\ red}$ (+/•)/V	$E^{2\ red}$ (•/−)/V
1a	[d]	−0.91	−0.78	−1.84
1b	−0.21[e,f]	−0.24	0.21	−1.28
1c	[d]	−0.66	−0.28	−1.64
1d	[d]	−0.67	−0.57	−1.64
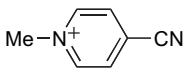	−0.52[g]	[h]	−0.32	−1.48

[a] Recorded in MeCN (0.1 M $[Bu_4N]^+[ClO_4]^-$) and reported relative to SCE.
[b] B3LYP/6-311+G(2d,p)//B3LYP/6-311G(2d,p) level as ΔH in MeCN dielectric medium.
[c] Cathodic peak potential.
[d] Irreversible process.
[e] Second cathodic wave at $E_{pc}^{2\ red}$=−0.89 V.
[f] lit. $E_{1/2}^{1\ red}$=−0.26 V and $E_{pc}^{2\ red}$=−1.10 V (0.1 M $[Et_4N]^+[ClO_4]^-$ in MeCN versus SCE) Ref. 8.
[g] $[Bu_4N]^+[ClO_4]^-$ (0.25 M) in MeCN versus Ag/Ag^+ (0.01 M in MeCN) assumed to be 0.44 V versus SCE. Ref. 26.
[h] Not reported.

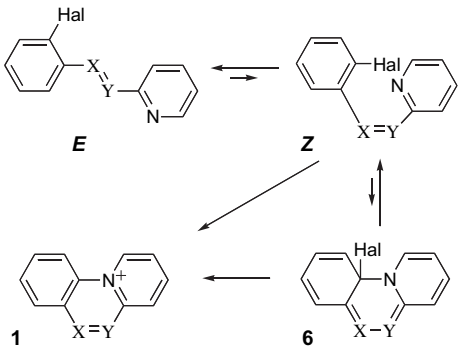

Scheme 3.

and ***Z*-IV** (**2d**, **3d**). This preference for conformational minimum is different in gas phase. Selected optimized structures involved in the transformation of **2b** and **3b** to **1b** are shown in Fig. 3.

but it was estimated at >40 kcal/mol. Analysis of the TS structures demonstrates that the cis–trans isomerization for the nitrogen-containing derivatives **2b**–**d** and **3b**–**d** proceeds through inversion at the N atom, which is consistent with previous computational results for phenylazopyridine[17] and *N*-benzylideneaniline.[18–20]

Results shown in Table 2 demonstrate that cis and trans forms interconvert thermally only for azomethine derivatives **c** and **d**. The barrier $\Delta G^{\ddagger}_{298}$ calculated for **3c** and **3d** is about 19 kcal/mol for the $E \rightarrow Z$ isomerization and is less than 12 kcal/mol for the reverse process. The analogous barriers to isomerization for the chloro derivatives **2c** and **2d** are higher by up to 5.6 kcal/mol calculated for **2d**-***Z*** → **2d**-***E***. For all four compounds the concentration of the cis isomers at the equilibrium is small, less than 0.1%. The calculated low activation energy for $Z \rightarrow E$ conversion is consistent with that experimentally established for isomerization of benzylideaniline (E_a=17.3 kcal/mol in MeCN)[21] and pyridyl phenyl azomethine (E_a=13.1–14.3 kcal/mol),[22] which are the closest experimental models of **c** and **d**.

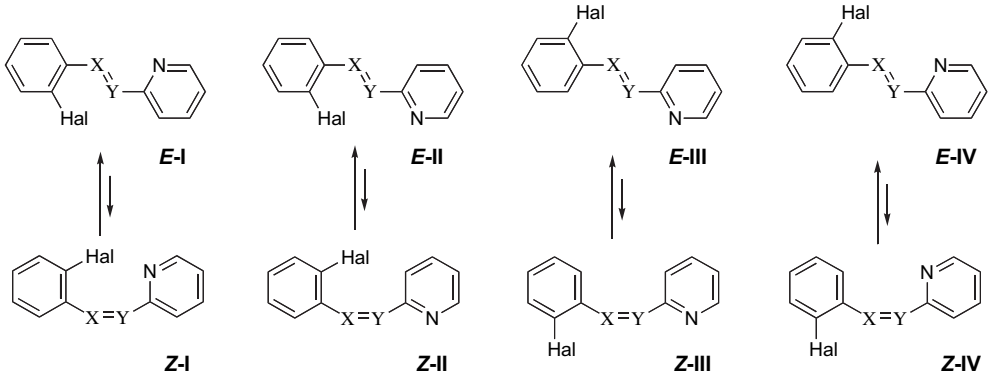

Fig. 2. Conformers of ***E*** and ***Z*** isomers.

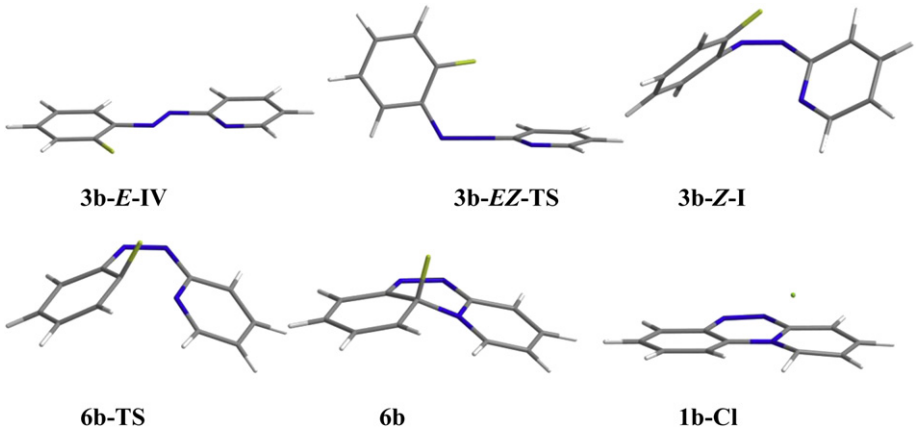

Fig. 3. B3LYP/6-311G(2d,p) optimized geometries for selected structures involved in cyclization **3b** to **6b** and **1-Cl** formed from **2-*Z*-I**.

All four conformers of **3a**-***E***, and also **2a**-***E*-I**, **2b**-***E*-III**, **2d**-***E*-IV**, and **3b**-***E*-III** converged to planar structures as confirmed by frequency calculations for C_s-constrained molecules. Surprisingly, fully optimized structure of one conformer of *cis* stilbazole, **3a**-***Z*-IV**, also has the C_s symmetry, apparently due to favorable C–H···N interactions (d=2.102 Å).

The energy difference between the cis and trans forms was calculated for the global minima of each isomer. For simplicity, the free energy of activation $\Delta G^{\ddagger}_{298}$ for the cis → trans isomerization was calculated for **2**-***Z*** and **3**-***Z*** global minimum conformers in MeCN (Table 2). The transition state structure for isomerization of stilbazoles **2a** and **3a** could not be located using standard methods,

Results for azenes **b** indicate that the cis isomers **2b**-***Z*** and **3b**-***Z*** cannot be thermally populated due to high $E \rightarrow Z$ isomerization barrier of $\Delta G^{\ddagger}_{298}$ >35 kcal/mol, but both cis forms can thermally isomerize to the more stable trans isomers **2b**-***E*** and **3b**-***E***. The calculated height of the barrier of $\Delta G^{\ddagger}_{298}$=24.5 kcal/mol (Table 2) in MeCN for the **2b**-***Z*** → **2b**-***E*** process is in good agreement with the experimental activation energy for phenylazopyridine ($\Delta G^{\ddagger}_{298}$=25.5 kcal/mol, $\Delta S^{\ddagger}$=−14.5 cal/molK).[23] The same barrier for the fluoro analogue is lower by nearly 7 kcal/mol. Finally, high barriers to isomerization estimated for stilbazoles **2a** and **3a** and established experimentally for Z-stilbene (E_a=42.8 kcal/mol)[24] prevent thermal isomerization of either **a**-***Z*** or **a**-***E***.

The intramolecular cyclization of halophenyl derivatives occurs form the **2**-*Z*-**I** and **3**-*Z*-**I** conformers and proceeds by an apparent 6π electrocyclic process. The former yields nearly planar cations with the chloride anion weakly coordinated to the C1 position (d_{C1Cl}=2.3 Å–2.5 Å) in **1**-**Cl**, while the cyclization of the later, fluorophenyl derivatives **3**-*Z*-**I**, leads to non-aromatic product **6**. The free energy of activation $\Delta G^{\ddagger}_{298}$ required for the cyclization of chlorophenyls **2**-*Z*-**I** is in a range of about 30 kcal/mol (**2b**-*Z*)–35 kcal/mol (**2c**-*Z*) and the reaction is exergonic by 18–24 kcal/mol. In contrast, cyclization of fluorophenyl **2**-*Z*-**I** to the non-aromatic **6** has lower activation barrier by 6–8 kcal/mol than that for the chloro analogues, but the process is significantly endergonic by 6–18 kcal/mol and thermally reversible. The least unfavorable cyclization is calculated for **3b**-*Z* (ΔG_{298}=5.7 kcal/mol), while the formation of **6a** and **6c** is most endergonic and requires additional 10.6 and 12 kcal/mol, respectively. This order of energies is consistent with that of the C–F distance in **6**: the shortest is found in **6b** (d_{CF}=1.446 Å) and the longest in **6a** (d_{CF}=1.471 Å).

The difference in behavior of the two halides presumably results from much better solvation of the chloride in organic media than that of F^-. As a consequence, the progress of the reaction of **3**-*Z* is 'frozen' at the stage of **6**, while reaction of chlorophenyl derivatives **2** progresses to the formation of cation **1**.

Computational data are consistent with experimental results, which demonstrate that only **1a**-**Cl** can be obtained thermally from **2a** in a metal-ion-free process. The cyclization reaction is exothermic and is faster than isomerization of **2a**-*Z* to **2a**-*E*. The later is also true for **3a**-*Z* but the reaction is significantly endothermic and the product is not formed. For the remaining chlorophenyl and fluorophenyl derivatives, the cis-to-trans isomerization reaction is faster than cyclization and no product formation is observed. In addition, cyclization reactions of fluorophenyl derivatives **2** are endothermic.

Experimental results of successful formation of cations **1** upon addition of Ag^+ to chlorides **2** and Ca^{2+} to fluorides **3** suggest that the ions coordinate to the halogens and significantly alter the potential energy surface for the cyclization and presumably for isomerization processes. The activation energy for cyclization of the coordinated halide becomes lower than that for isomerization, and consequently formation of **1** is faster for halides **2** and **3**.

The formation of the requisite cis isomers of the Schiff bases, **3c**-*Z* and **3d**-*Z*, is accomplished thermally, which, in accordance with the computational results, shows that the two isomers are in thermal equilibrium. The generation of **2b**-*Z* and **3b**-*Z* isomers in concentrations sufficient for efficient formation cyclization requires intense light, since both thermally convert to **2b**-*E* and **3b**-*E* and neither can be transformed thermally back to the cis forms. Finally, the preparation of **1a** requires I_2 catalysis at high temperature to equilibrate the **a**-*E* and **a**-*Z* forms. Without the catalyst the requisite **2a**-*Z* and **3a**-*Z* isomers are thermally inaccessible from the trans forms. However, both can be obtained photochemically.[1]

2.5. NMR chemical shift assignment

Structural assignment of ^1H and ^{13}C signals in cations **1** was accomplished by taking advantage of peak multiplicity, by analysis of 2-D (^1H–^1H and ^1H–^{13}C) and DEPT-90 NMR spectra recorded in DMSO-d_6 solutions,[25] and by using DFT-calculated ^{13}C chemical shifts in the solvent's dielectric medium. In all four cations the assignment started from the highly deshielded proton appearing as a doublet at the C(1) carbon atom adjacent to the pyridinium nitrogen atom. Assignment for the benzene ring was helped by DFT results showing that the C(10) carbon atom is the most shielded in the molecule and appears at about 115 ppm in the spectrum. The quaternary carbon atoms, C(4a), C(6a), and C(10a), were identified by DEPT-90 technique and assigned according to the DFT results. Computational results also helped with the assignment of the resonance to the C(5) and C(6) nuclei in **1a**. Assigned experimental and calculated chemical shifts are shown in Table 3.

A comparison of the computed chemical shifts with experimental values in Table 3 demonstrates a close agreement for the ^{13}C nuclei. The mean difference between experimental and theoretical values is −0.6±2.0 ppm (absolute 1.7±1.1 ppm). The largest differences $\Delta\delta$ between experiment and theory are observed for the C(1) carbon in all cations ($\Delta\delta$ >3 ppm), and for C(7) in **1b** ($\Delta\delta$=−4.1 ppm). ^1H NMR chemical shifts are less accurately predicted and larger differences $\Delta\delta$ are observed especially for the C(1)–H nuclei for which $\Delta\delta$ values are in a range of 0.59–0.74 ppm. The mean deviation for all ^1H NMR datapoints is 0.23±0.21 ppm (absolute 0.25±0.19 ppm), while without the C(1)–H nuclei it improves to 0.18±0.16 ppm (absolute 0.20±0.13 ppm).

2.6. Electronic spectra

Experimental absorption and emission spectra for salts **1a**[ClO_4]–**1d**[ClO_4] were recorded in MeCN and selected data are presented in Fig. 4 and Table 4.

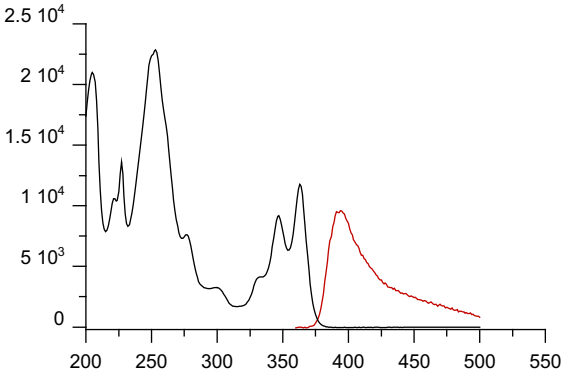

Fig. 4. Absorption (black) and emission (red, λ_{ex}=347 nm) spectra for **1a**[ClO_4] recorded in MeCN.

All four cations exhibit moderate absorption in the region of about 340 nm and significantly stronger absorption at about 260 nm. The low energy absorption exhibits vibronic structure with the splitting of about 1330 cm^{-1} for **1a** and **1d** and about 950 cm^{-1} for **1b**. Table 4 lists the (0,0) transitions for the cations. Two of the four cations fluoresce at ambient temperature. Thus, solutions of **1a**[ClO_4] and **1c**[ClO_4] in MeCN exhibit a moderate fluorescence with a maximum at 394 nm (λ_{ex}=347 nm). Despite efforts, fluorescence that was reported[8] for **1b** at 535 nm was not observed even for a wide range of excitation wavelengths.

To shed more light on the nature and origin of the observed transitions, we conducted TD DFT calculation in MeCN dielectric medium. Calculations demonstrated that there are three main π–π* excitations of moderate intensity in a range of about 340 nm, 270 nm, and 250 nm. This is consistent with experimental spectra assuming that the two high energy excitations are merged into a broad absorption band observed e.g., at 257 nm for **1a** (Fig. 1). The lowest energy excitation involves transition mainly from the HOMO to the LUMO, both orbitals delocalized over the entire molecule as shown for **1d** in Fig. 5. The higher energy excitation involves HOMO→LUMO+1 and HOMO-1→LUMO as the main transitions in **1a** and **1d**. The excitation in **1b** at 286 nm involves HOMO-2→LUMO, since HOMO-1 is A′ symmetry orbital and contains the lone pairs. In cation **1c**, this medium energy excitation is apparently split into two bands: one at 329 nm involving the HOMO-1→LUMO transition, and the second at 286 nm originating from the HOMO-→LUMO+1 transition. The next highest π–π* excitation at about

250 nm involves the HOMO-1→LUMO+1 transition for **1a**, **1c**, and **1d**, and HOMO-2→LUMO+1 transition for **1b**.

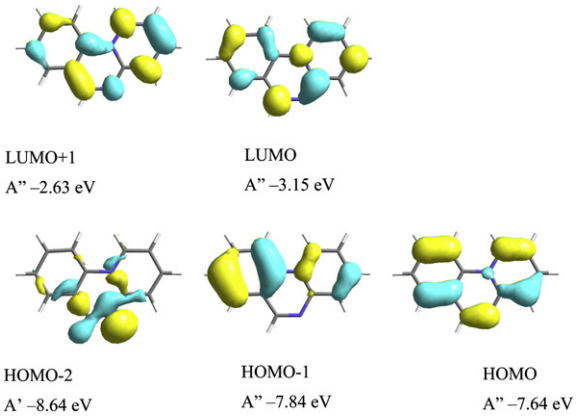

Fig. 5. B3LYP/6-311+G(2d,p) derived contours and energies of molecular orbitals relevant to low energy excitations for **1d** in MeCN dielectric medium.

The non-bonding electrons of the nitrogen atoms constitute the HOMO-1 in **1b** and HOMO-2 in **1c** and **1d** (Fig. 5). The forbidden n–π* excitation for **1b** is predicted at 429 nm and 310 nm, which is consistent with the observed low intensity absorption band tailing to about 450 nm. The n–π* excitations in **1c** and **1d** are calculated at 311 nm and 288 nm, respectively, and presumably are obscured by the more intense π–π* bands.

2.7. Reduction of cations 1

One electron reduction of cations **1** leads to π-delocalized heteroaromatic radicals **1•** (Scheme 4), which are analogues of pyridyl radicals obtained from pyridinium salts.[26] Further reduction of the radicals results in anions $\mathbf{1}^-$ (Scheme 4). The formation and stability of these species was studied electrochemically and computationally.

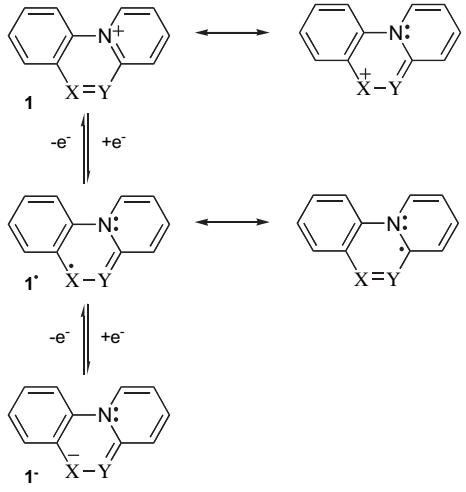

Scheme 4.

Cyclic voltammetry analysis demonstrated that only **1b** exhibits reversible reduction wave at $E_{1/2}$=−0.21 V and irreversible cathodic wave at −0.89 V (Table 5). The remaining three cations undergo irreversible +/• reduction at lower potentials; 0.4 V lower for cations containing one bridging nitrogen, **1c** and **1d**, and nearly 0.7 V lower for **1a**. The experimental order of reduction potentials, **1b**>**1d**~**1c**>**1a**, is similar to that established computationally **1b**>**1c**>**1d**>**1a** (Table 5) and reflects the ability to stabilize the positive charge in the cations. Potentials for reduction of radicals **1•** to anions $\mathbf{1}^-$ (•/−) are calculated to be over 1 V more cathodic. A comparison to the pyridinium derivatives demonstrates that **1b** is easier to reduce than 4-cyano-*N*-methylpyridinium[26] by about 0.3 V, which in turn is about 0.15 V more anodic than reduction of **1c** and **1d**.

Analysis of radicals **1•** demonstrates that spin is localized mainly on the central ring with the most significant spin concentration on the X(6) atom, while relatively little spin is delocalized onto the benzene ring (Fig. 6). This is consistent with the major resonance forms of the radicals shown in Scheme 4. A relatively high positive spin density is localized at the C(3) position and suggests a potential substitution site that may help to stabilize the radical. Radicals **1b•** and **1c•** in which the spin is stabilized by the N(6) atom are planar. All anions are found to be non-planar.

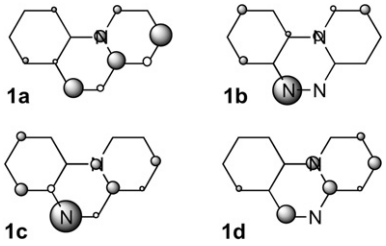

Fig. 6. Calculated spin density for radical **1•** at the B3LYP/6-311+G(2d,p)//B3LYP/6-311G(2d,p) level of theory in MeCN dielectric medium. Dark circles represent positive values. For details see Supplementary data.

A comparison of computational results for the two isomeric species **c** and **d** demonstrates that cation **1d** is more thermodynamically stable than **1c** by 2.9 kcal/mol, while radical **1c•** is more stable than **1d•** by 3.4 kcal/mol in MeCN dielectric medium. The former reflects better stabilization of the positive charge by the C(6) carbon atom delocalized from the pyridinium, while the unpaired electron in **1•** is better accommodated by the nitrogen atom in the same position (Scheme 4).

3. Conclusions

Results demonstrate that cations **1a**–**d** are accessible from fluoro derivatives **3** by Ca^{2+}-promoted cyclization. The process involves trans-to-cis isomerization of **3** followed by Ca^{2+}-assisted electrocyclization to cation **1**. In the absence of Ca^{2+} ions cyclization of ***3-Z*** leads to an endothermic intermediate **6** through a barrier higher (for **b**–**d**) than that for isomerization to ***3-E***, according to DFT calculations. The reaction conditions, such as the use of heat or light to populate the less thermodynamically stable cis isomer ***3-Z*** necessary for the cyclization, are consistent with the calculated barriers for isomerization.

A comparison of the experimental and theoretical molecular structures for three of the four cations demonstrated that the B3LYP method with the 6-311G(2d,p) basis set particularly well reproduces the experimental geometry and provides a tool for assessing formation and properties of this class of organic cations. The DFT method was used successfully to assign NMR chemical shifts, analysis of electronic absorption spectra, and study of reduction of cations **1** to radicals **1•**. In general, experimental results were well reproduced by DFT calculations.

Spectroscopic analysis demonstrated that all four cations exhibit two main regions of absorption at about 350 nm and 260 nm related to π–π* excitation. Among the cations only **1a** and **1c** exhibit fluorescence with a maximum at about 394 nm. Fluorescence reported for **1b** was not confirmed.

Electrochemical analysis revealed that only **1b** exhibits reversible (+/•) reduction with half potential of −0.21 V, while the remaining three cations undergo irreversible reduction at more

cathodic potentials. Substitution at high spin density site C(3) with an electron-withdrawing group may lead to stabilization of the radicals and reversible reduction of the cations.

The sequential introduction of the nitrogen atoms to the X(6)–Y(5) bridge of **1a** has a significant effect on electrochemical behavior of the cation, but much less on their photophysical properties. Interestingly, the position of the nitrogen atom in the bridge has effect on photoluminescence properties, relative stability, and the energy profile for the formation of the two isomeric cations from **3c** and **3d**.

Overall, the results demonstrate a potentially general method for the preparation of heterocyclic cations, analogues of **1a**–**d**, and derivatives that are suitable for incorporation into more complex molecular architectures. The developed computational protocol permits the design of new cations and evaluation of their formation and properties.

4. Computational details

Quantum-mechanical calculations were carried out with the B3LYP[27,28] and MP2(fc)[29] methods with 6-31G(d,p), 6-311G(2d,p), 6-31+G(2d,p), or cc-pVDZ basis set using the Gaussian 03 and Gaussian 09 packages.[30,31] Geometry optimizations were undertaken using appropriate symmetry constraints and tight convergence limits. Vibrational frequencies were used to characterize the nature of the stationary points achieved with the DFT method, and to obtain thermodynamic parameters. Zero-point energy (ZPE) corrections were scaled by 0.9806.[32] Geometry optimizations at the MP2 level were initially performed without symmetry constraints, and the resulting planar structures were reoptimized with the imposed C_s symmetry.

Electronic excitation energies for cations **1** were obtained at the B3LYP/6-311+G(2d,p)//B3LYP/6-311G(2d,p) level using the time-dependent DFT calculations[33] supplied in the Gaussian package. Solvent effect on electronic excitations was included using the PCM model[34] [keywords: SCRF(PCM, Solvent=CH_3CN)].

NMR shielding tensors for **1** were obtained at the B3LYP/6-311+G(2d,p)//B3LYP/6-311G(2d,p) level using the GIAO method[35] and solvent effects were included using keywords: SCRF(PCM, Solvent=DMSO). The computed isotropic shielding parameters for **1** were referenced using chemical shift of benzene calculated at the same level of theory and experimentally observed[36] in DMSO-d_6 (7.37 ppm for ^{1}H and 128.3 ppm for ^{13}C).

Reduction potentials E^0 were based on energies calculated for cations **1**, radicals **1**$^{\bullet}$, and anions **1**$^-$ at the B3LYP/6-311+G(2d,p)//B3LYP/6-311G(2d,p) level of theory with tight convergence criteria in MeCN dielectric medium using the IPCM model[37] (keywords: SCRF=IPCM) and epsilon value of 36.64. The free energies calculated with thermodynamic corrections derived from B3LYP/6-311G(2d,p) calculations were converted to volts using the expression $\Delta G(\mathrm{sol}) = -FE^0$ where F is the Faraday constant, and correcting by 4.189 V for the difference between the absolute potential for standard hydrogen electrode (SHE, 4.43 V)[38] and SCE electrode relative to SHE (0.241 V).

Mechanistic studies were conducted at the B3LYP/6-311G(2d,p) level of theory with tight convergence criteria. Global conformational minima for each trans and cis isomers, **3**-**E** and **3**-**Z**, were established by comparison of SCF energies for four conformers at fully optimized geometries without symmetry constraints. Transition state structures for cis–trans isomerization and formation of **6** were located using the STQN method[39] requested with the QST2 keyword and default convergence criteria. Final energies for each optimized structure were calculated with the B3LYP/6-311+G(2d,p)//B3LYP/6-311G(2d,p) method and inclusion of solvation effects requested with the SCRF=IPCM keyword (epsilon=36.64).

5. Experimental section

5.1. General remarks

Melting points are uncorrected. NMR spectra were recorded at 400 or 500 MHz (^{1}H), and 75 or 100 MHz (^{13}C), respectively, in $CDCl_3$ (7.26 and 77.0 ppm), CD_3CN (1.95 ppm), anhydrous DMSO-d_6 (2.49 and 39.5 ppm) as specified. DMSO-d_6 was taken from freshly opened ampule. Chemical shifts were referenced to TMS (^{1}H) or solvent (^{13}C). UV spectra were recorded in spectroscopic-grade CH_3CN. Molar extinction coefficients were obtained by fitting maximum absorbance against concentration in agreement with Beer's law.

5.2. Photocyclization

Solutions of halide **2** or **3** were placed in a Pyrex NMR tube or flask and irradiated without filter with a Husky work light (WL500SPC-H) setup equipped with a 500 W (125–130 V) clear halogen double ended lamp (T3 base) at a distance of about 50 cm. The reaction mixtures were spontaneously heated up by the lamp.

5.3. Cyclic voltammetry

Electrochemical analysis of **1**[$\mathbf{ClO_4}$] was conducted under dry argon in MeCN (distilled over CaH_2) containing freshly dried $[Bu_4N]^+[ClO_4]^-$ (50 °C, P_2O_5, vacuum, overnight) as the supporting electrolyte (0.1 M) and Pt microdisk working electrode with Ag/AgCl pseudoelectrode as reference. The concentration of **1**[$\mathbf{ClO_4}$] was about 1 mM and the scanning rate was 0.1 V/s. Peak potentials were referenced to the Fc/Fc$^+$ couple by adding small amounts of ferrocene to the solution, which was assumed to be +0.462 V versus SCE (MeCN, 0.1 M $[Bu_4N]^+[ClO_4]^-$).[40]

*5.3.1. Benzo[c]quinolizinium perchlorate (**1a**[**ClO$_4$**])[1].* A mixture of **2a** (250 mg, 1.1 mmol) and catalytic amounts of I_2 was refluxed in dry benzonitrile (5 mL) for 36 h. The solvent was removed in vacuum, the residue was dissolved in water, insoluble brown solid was filtered, and 70% aqueous $HClO_4$ was added to the filtrate. The resulting pale yellow solid was filtered, washed with water and Et_2O, and recrystallized (EtOH) to afford 150 mg (54% yield) of **1a**[$\mathbf{ClO_4}$] as yellowish crystals: mp 195–197 °C (lit.[1] mp 187–189 °C); ^{1}H NMR (400.1 MHz, CD_3CN) δ 8.06 (td, J_1=7.6 Hz, J_2=0.7 Hz, 1H), 8.15–8.22 (m, 2H), 8.18 (d, J=9.0 Hz, 1H), 8.32 (dd, J_1=8.0 Hz, J_2=1.5 Hz, 1H), 8.49–8.57 (m, 2H), 8.58 (d, J=9.2 Hz, 1H), 8.83 (d, J=9.0 Hz, 1H), 9.96 (d, J=7.0 Hz, 1H); ^{1}H NMR (500 MHz, DMSO-d_6) δ 8.08 (t, J=7.5 Hz, 1H), 8.21 (td, J_1=8.0 Hz, J_2=1.6 Hz, 1H), 8.28 (td, J_1=7.0 Hz, J_2=1.8 Hz, 1H), 8.39 (d, J=9.0 Hz, 1H), 8.40 (dd, J_1=7.9 Hz, J_2=1.5 Hz, 1H), 8.66 (td, J_1=7.7 Hz, J_2=0.9 Hz, 1H), 8.71 (dd, J_1=8.3 Hz, J_2=1.6 Hz, 1H), 8.74 (d, J=9.0 Hz, 1H), 9.16 (d, J=8.9 Hz, 1H), 10.39 (d, J=7.0 Hz, 1H); ^{13}C NMR (75.5 MHz, DMSO-d_6, DEPT 90) δ 118.0, 122.9, 124.3, 126.8 (q), 128.4, 130.4, 130.5, 132.8, 134.2 (q), 134.6, 136.6, 140.5, 143.3 (q); UV (CH_3CN), λ_{max} (log ϵ) 222 (4.13), 227 (4.24), 253 (4.47), 277 (3.99), 299 (3.62), 332 (3.72), 347 (4.07), 363 (4.18) nm [lit.[3] (EtOH) λ_{max} (log ϵ) 228 (3.85), 255 (4.07), 348 (3.68), 365 (3.80) nm]. Anal. Calcd for $C_{13}H_{10}ClNO_4$: C, 55.83; H, 3.60; N, 5.01. Found: C, 55.83; H, 3.47; N, 4.99.

*5.3.2. Pyrido[2,1-c][1,2,4]benzotriazin-11-ium p-toluenosulfonate (**1b**[**OTs**]).* 2-(2-Fluorophenylazo)pyridine (**3b**, 201 mg, 1.0 mmol) and calcium *p*-toluenosulfonate (190 mg, 1.0 mmol) were dissolved in a MeCN/H_2O mixture (9:1, 30 mL). The resulted solution was irradiated with a halogen lamp and refluxed during 1–1.5 h (until TLC control showed reaction was completed). Then, solvents were evaporated. Residue was dried in a desiccator over P_2O_5 (12 h). The solid was suspended in CH_2Cl_2 and filtered. Subsequently, it was

dissolved in hot MeCN, solution filtered, and the solvent was evaporated to give a yellow-green solid. The product was recrystallized (toluene/MeCN) to give 250 mg (85% yield) of **1b**[**OTs**] as green-black crystals: mp 244–246 °C; ^{1}H NMR (CD_3CN) δ 2.31 (s, 3H), 7.12 (d, J = 7.9 Hz, 2H), 7.56 (d, J = 8.0 Hz, 2H), 8.37 (t, J = 8.0 Hz, 1H), 8.51 (t, J = 8.6 Hz, 1H), 8.59 (t, J = 7.0 Hz, 1H), 8.92 (d, J = 8.7 Hz, 1H), 9.08-9.03 (m, 2H), 9.27 (d, J = 8.4 Hz, 1H), 10.08 (d, J = 6.6 Hz, 1H); ^{13}C NMR (75.5 MHz, DMSO-d_6, DEPT 90) δ 20.8 (CH_3), 116.9, 123.2 (q), 125.4, 128.0, 129.2, 130.4, 132.2, 137.6 (q), 138.8, 141.4 (q), 142.4 (q), 145.6 (q), 146.0. Anal. Calcd for $C_{18}H_{15}N_3O_3S$: C, 61.18; H, 4.28; N, 11.89. Found: C, 60.73; H, 4.12; N, 11.96.

*5.3.3. Pyrido[2,1-c][1,2,4]benzotriazin-11-ium perchlorate (**1b**[**ClO$_4$**])*[8]. Triazinium *p*-toluenosulfonate **1b**[**TsO**] (100 mg, 0.28 mmol) was dissolved in water (2 mL) and excess of satd solution of $NaClO_4$ was added. The resulting precipitation was filtrated to give 48 mg (61% yield) of brown-red crystals: mp >295 °C; ^{1}H NMR (400 MHz, CD_3CN) δ 8.41 (d, J = 7.7 Hz, 1H), 8.53 (td, J_1 = 8.7 Hz, J_2 = 1.4 Hz, 1H), 8.60 (t, J = 6.3 Hz, 1H), 8.86 (d, J = 8.7 Hz, 1H), 9.08 (t, J = 7.6 Hz, 1H), 9.30 (d, J = 8.4 Hz, 1H), 9.97 (d, J = 6.7 Hz, 1H); ^{1}H NMR (500 MHz, DMSO-d_6) δ 8.42 (td, J_1 = 8.0 Hz, J_2 = 0.6 Hz, 1H), 8.60 (td, J_1 = 8.7 Hz, J_2 = 1.4 Hz, 1H), 8.74 (td, J_1 = 7.6 Hz, J_2 = 1.5 Hz, 1H), 9.13 (dd, J_1 = 8.1 Hz, J_2 = 1.3 Hz, 1H), 9.18 (td, J_1 = 8.94, Hz, J_2 = 1.1 Hz, 1H), 9.23 (d, J = 8.7 Hz, 1H), 9.46 (dd, J_1 = 6.9 Hz, J_2 = 2.1 Hz, 1H), 10.50 (d, J = 6.6 Hz, 1H); ^{13}C NMR (75.5 MHz, DMSO-d_6, DEPT 90) δ 116.8, 123.1 (q), 129.2, 130.5, 132.3, 133.0, 133.3, 138.9, 141.4 (q), 142.4 (q), 146.0; UV (CH_3CN), λ_{max} (log ϵ) 259 (4.32), 347 (3.87), 359 (3.88) [lit.[8] (CH_3CN), λ_{max} (log ϵ) 258 (4.37), 348 (3.90), 359 (3.91), 375 sh (3.73)]. Anal. Calcd for $C_{11}H_8ClN_3O_4$: C, 46.91; H, 2.86; N, 14.92. Found: C, 47.04; H, 2.78; N, 14.70.

*5.3.4. Pyrido[1,2-a]quinoxalin-11-ium perchlorate (**1c**[**ClO$_4$**]).* Using a procedure similar to that described for **1d**[**ClO$_4$**], salt **1c**[**ClO$_4$**] was prepared in 12% yield from **3c** as red crystals: mp 246–248 °C; ^{1}H NMR (400 MHz, CD_3CN) δ 8.15–8.23 (m, 2H), 8.43–8.47 (m, 1H), 8.52 (td, J_1=7.0 Hz, J_2=1.6 Hz, 1H), 8.78–8.83 (m, 2H), 8.87 (td, J_1=7.7 Hz, J_2=1.0 Hz, 1H), 9.66 (s, 1H), 10.05 (d, J=6.8 Hz, 1H); ^{1}H NMR (500 MHz, DMSO-d_6) δ 8.18 (td, J_1=7.5 Hz, J_2=1.1 Hz, 1H), 8.22 (td, J_1=7.2 Hz, J_2=1.6 Hz, 1H), 8.44 (dd, J_1=7.8 Hz, J_2=1.7 Hz, 1H), 8.64 (td, J_1=6.9 Hz, J_2=2.1 Hz, 1H), 8.99 (td, J_1=8.0 Hz, J_2=0.7 Hz, 1H), 9.01 (dd, J_1=8.0 Hz, J_2=2.0 Hz, 1H), 9.15 (d, J=8.3 Hz, 1H), 9.88 (s, 1H), 10.54 (d, J=6.7 Hz, 1H); ^{13}C NMR (75.5 MHz, DMSO-d_6, DEPT 90) δ 117.7, 126.7 (q), 128.7, 129.1, 131.2, 132.4, 132.5, 134.4 (q), 134.9, 139.2 (q), 143.7, 150.6; UV (CH_3CN), λ_{max} (log ϵ) 226 (4.08), 242 (4.14), 256 (4.25), 317 (3.50), 331 (3.72), 346.5 (3.99), 363.5 (4.07) nm. Anal. Calcd for $C_{12}H_9ClN_2O_4$: C, 51.35; H, 3.23; N, 9.98. Found: C, 51.18; H, 3.09; N, 9.97.

*5.3.5. Pyrido[1,2-a]quinazolin-11-ium perchlorate (**1d**[**ClO$_4$**]).* A mixture of imine **3d** (3.80 g, 19.0 mmol) and $Ca(OTs)_2$ (3.20 g, 8.4 mmol) in dry PhCN (60 mL) was heated at 160 °C for 3 h. The solvent was removed at reduced pressure and the residue was dissolved in water. An insoluble black solid was filtered, the aqueous filtrate was heated with activated carbon, filtered, concentrated in vacuum and excess of satd solution of $NaClO_4$ was added. The resulting precipitation was filtered and dried to give 1.23 g (18% yield) of **1d**[**ClO$_4$**] as red crystals. An analytically pure sample was obtained by recrystallization of the salt from EtOH and then from MeCN: mp 244–246 °C; ^{1}H NMR (400 MHz, CD_3CN) δ 8.21 (td, J_1=7.6 Hz, J_2=0.5 Hz, 1H), 8.25 (td, J_1=7.1 Hz, J_2=1.5 Hz, 1H), 8.45 (ddd, J_1=8.9 Hz, J_2=7.3 Hz, J_3=1.5 Hz, 1H), 8.53 (dd, J_1=7.9 Hz, J_2=1.4 Hz, 1H), 8.59 (dd, J_1=8.4 Hz, J_2=1.2 Hz, 1H), 8.74 (ddd, J_1=8.5 Hz, J_2=7.3 Hz, J_3=1.3 Hz, 1H), 8.83 (d, J=8.9 Hz, 1H), 9.80 (s, 1H), 9.86 (d, J=6.9 Hz, 1H); ^{1}H NMR (500 MHz, DMSO-d_6) δ 8.23 (t, J=7.5 Hz, 1H), 8.36 (td, J_1=7.0 Hz, J_2=1.2 Hz, 1H), 8.49 (td, J_1=8.0 Hz, J_2=1.1 Hz, 1H), 8.63 (d, J=7.9 Hz, 1H), 8.68 (d, J=8.4 Hz, 1H), 9.17 (d, J=8.9 Hz, 1H), 10.00 (s, 1H), 10.32 (d, J=6.8 Hz, 1H); ^{13}C NMR (75.5 MHz, DMSO-d_6, DEPT 90) δ 117.4, 121.9 (q), 124.6, 129.0, 130.8, 131.5, 134.1, 135.9 (q), 137.6, 144.2, 147.6 (q), 162.5; UV (CH_3CN), λ_{max} (log ϵ) 222 (4.01), 250 (4.54), 266 sh (4.23), 306 (3.66), 319 (3.77), 333.5 (3.98), 349 (4.04) nm. Anal. Calcd for $C_{12}H_9ClN_2O_4$: C, 51.35; H, 3.23; N, 9.98. Found: C, 51.44; H, 3.34; N, 9.98.

*5.3.6. trans-2-[2-(Chlorophenyl)vinyl]pyridine (**2a**)*[1]. A mixture of 2-picoline (3.0 g, 32.30 mmol) and 2-chlorobenzaldehyde (4.74 g, 33.70 mmol) was refluxed in acetic anhydride (6 mL) for 20 h under Ar atmosphere. Acetic anhydride was removed under vacuum, a mixture of cyclohexane and EtOAc (1:1, 20 mL) was added, the resulting solution was washed with satd $NaHCO_3$, dried (Na_2SO_4), and the solvents were evaporated. The crude product was purified using a silica gel plug (CH_2Cl_2) and subsequent recrystallization from hexane to give 4.73 g (69% yield) of **2a** as pale yellow crystals: mp 78–79 °C (lit.[1] mp 75–76.6 °C); ^{1}H NMR (400 MHz, $CDCl_3$) δ 7.17 (d, J=16.1 Hz, 1H), 7.15–7.20 (m, 1H), 7.23 (td, J_1=7.7 Hz, J_2=1.8 Hz, 1H), 7.29 (td, J_1=7.4 Hz, J_2=1.4 Hz, 1H), 7.41 (dd, J_1=7.8 Hz, J_2=1.4 Hz, 1H), 7.47 (d, J=7.9 Hz, 1H), 7.68 (td, J_1=7.7 Hz, J_2=1.8 Hz, 1H), 7.73 (dd, J_1=7.7 Hz, J_2=1.8 Hz, 1H), 7.98 (d, J=16.2 Hz, 1H), 8.63 (dd, J_1=4.8 Hz, J_2=0.8 Hz, 1H); ^{1}H NMR (500 MHz, CD_3CN) δ 7.24–7.27 (m, 1H), 7.28 (d, J=16.0 Hz, 1H), 7.31 (td, J_1=7.6 Hz, J_2=1.7 Hz, 1H), 7.37 (td, J_1=7.9 Hz, J_2=0.7 Hz, 1H), 7.470 (d, J=8.9 Hz, 1H), 7.474 (d, J=8.9 Hz, 1H), 7.76 (td, J_1=7.7 Hz, J_2=1.8 Hz, 1H), 7.86 (dd, J_1=7.8 Hz, J_2=1.5 Hz, 1H), 8.07 (d, J=15.7 Hz, 1H), 8.61 (d, J=4.2 Hz, 1H).

*5.3.7. 2-(2-Chlorophenylazo)pyridine (**2b**)*[12]. To the solution of 2-aminopyridyne, (67 mg, 0.7 mmol) in toluene (0.1 mL), a solution of NaOH (50% in water, 0.7 mL) followed by 2-chloronitrosobenzene (102 mg, 0.7 mmol) was added. The mixture was vigorously stirred with mechanic stirrer for 25 min at 50 °C. After cooling, water was added and mixture was extracted with CH_2Cl_2, combined extracts were dried (Na_2SO_4), and the solvents were evaporated. The residue was purified using a silica gel plug (hexane/CH_2Cl_2, 5:1) followed by recrystallization from hexane to give 69 mg (61% of yield) of **2b** as red crystals: mp 52–54 °C; (lit.[12] mp 54–55 °C); ^{1}H NMR ($CDCl_3$) δ 8.77 (m, 1H), 7.94–7.84 (m, 3H), 7.58 (d, J=8.0 Hz, 1H), 7.49–7.42 (m, 2H), 7.36 (t, J=7.9 Hz, 1H).

*5.3.8. trans-2-[2-(Fluorophenyl)vinyl]pyridine (**3a**)*[11]. Prepared similarly to **2a**, **3a** was obtained in 34% yield as brown-yellow crystals: mp 74–76 °C (lit.[11] mp 71–72 °C); ^{1}H NMR (400 MHz, $CDCl_3$) δ 7.09 (ddd, J_1=10.8 Hz, J_2=8.2 Hz, J_3=1.1 Hz, 1H), 7.16 (br d, J=7.5 Hz, 1H), 7.15–7.19 (m, 1H), 7.23–7.28 (m, 1H), 7.28 (d, J_1=16.4 Hz, 1H), 7.43 (br d, J=7.9 Hz, 1H), 7.64 (td, J_1=7.7 Hz, J_2=1.7 Hz, 1H), 7.67 (td, J_1=7.8 Hz, J_2=1.8 Hz, 1H), 7.76 (d, J=16.3 Hz, 1H), 8.62 (dd, J_1=4.8 Hz, J_2=0.8 Hz, 1H); ^{1}H NMR (500 MHz, CD_3CN) δ 7.17 (dd, J_1=10.8 Hz, J_2=8.6 Hz, 1H), 7.21–7.26 (m, 1H), 7.24 (d, J=7.6 Hz, 1H), 7.32–7.38 (m, 1H), 7.34 (d, J=16.2 Hz, 1H), 7.48 (d, J=7.8 Hz, 1H), 7.75 (dd, J_1=7.7 Hz, J_2=1.7 Hz, 1H), 7.78 (dd, J_1=7.7 Hz, J_2=1.5 Hz, 1H), 7.83 (d, J=16.2 Hz, 1H), 8.60 (d, J=4.4 Hz, 1H).

*5.3.9. 2-(2-Fluorophenylazo)pyridine (**3b**).* Prepared similarly to that for **2b**, **3b** was obtained in 71% yield as red crystals: mp 52–54 °C; ^{1}H NMR ($CDCl_3$) δ 8.76 (dm, J=5.1 Hz, 1H), 7.94–7.83 (m, 3H), 7.56–7.49 (m, 1H), 7.43 (t, J=6.2 Hz, 1H), 7.33–7.22 (m, 2H); ^{13}C NMR (75.5 MHz, $CDCl_3$, DEPT 90) δ 114.2, 117.1 (d, J=20 Hz), 117.8, 124.3 (d, J=4 Hz), 125.5, 133.3 (d, J=9 Hz), 138.3, 140.2 (q), 149.5, 160.7 (q, J=260 Hz), 163.0 (q). Anal. Calcd for $C_{11}H_8FN_3$: C, 65.67; H, 4.01; N, 20.88. Found: C, 65.88; H, 4.07; N, 20.62.

*5.3.10. 2-Fluoro-N-(pyridin-2-ylmethylene)aniline (**3c**).* Using analogous procedure described for **3d**, imine **3c** was prepared in 55% yield as pale yellow crystals: mp 50–51 °C; ^{1}H NMR (400 MHz, $CDCl_3$) δ 7.13–7.25 (m, 4H), 7.39 (ddd, J_1=7.5 Hz, J_2=4.8 Hz, J_3=1.2 Hz, 1H), 7.83 (td, J_1=7.7 Hz, J_2=1.5 Hz, 1H), 8.27 (d, J=7.9 Hz, 1H), 8.67 (s,

1H), 8.72 (dq, J_1=4.8 Hz, J_2=0.9 Hz, 1H); ^{13}C NMR (75 MHz, $CDCl_3$) δ 116.3 (d, $^2J_{CF}$=20 Hz), 121.7, 121.9, 124.5 (d, $^4J_{CF}$=4 Hz), 125.4, 127.5 (d, $^3J_{CF}$=8 Hz), 136.6, 139.0 (q) (d, $^3J_{CF}$=10 Hz), 149.6, 154.3, 155.3 (d, $^1J_{CF}$=250 Hz), 163.0. Anal. Calcd for $C_{12}H_9FN_2$: C, 71.99; H, 4.53; N, 13.99. Found: C, 72.23; H, 4.48; N, 14.06.

*5.3.11. 2-(2-Fluorobenzylidenamino)pyridine (**3d**).* A mixture of 2-fluorobenzaldehyde (136 mg, 1.1 mmol), 2-aminopyridine (94 mg, 1 mmol), and TsOH (cat.) in benzene (5 mL) was refluxed for 4 h, the cooled solution was washed with satd $NaHCO_3$, dried ($NaSO_4$), and solvents were evaporated. The crude mixture was recrystallized (hexane) to give 135 mg (68% yield) of **3d** as pale yellow crystals: mp 120–122 °C; ^{1}H NMR (400 MHz, $CDCl_3$) δ 7.12–7.17 (m, 1H), 7.19 (ddd, J_1=7.3 Hz, J_2=4.9 Hz, J_3=0.9 Hz, 1H), 7.25 (t, J=7.6 Hz, 1H), 7.34 (d, J=8.0 Hz, 1H), 7.45–7.52 (m, 1H), 7.76 (td, J_1=7.7 Hz, J_2=1.9 Hz, 1H), 8.25 (td, J_1=7.5 Hz, J_2=1.7 Hz, 1H), 8.51 (dd, J_1=4.8 Hz, J_2=1.1 Hz, 1H), 9.45 (s, 1H); ^{13}C NMR (75.5 MHz, $CDCl_3$, DEPT-90) δ 115.9 (d, $^2J_{CF}$=21 Hz), 119.7, 122.0, 123.6(q) (d, $^2J_{CF}$=9 Hz), 124.3 (d, $^3J_{CF}$=4 Hz), 128.1 (d, $^4J_{CF}$=2 Hz), 133.5 (d, $^3J_{CF}$=9 Hz), 138.0, 148.9, 156.2 (d, $^3J_{CF}$=5 Hz), 161.0(q), 163.3 (d, $^1J_{CF}$=255 Hz). Anal. Calcd for $C_{12}H_9FN_2$: C, 71.99; H, 4.53; N, 13.99. Found: C, 71.86; H, 4.67; N, 13.99.

*5.3.12. 2-Chloronitrosobenzene (**4**)*[12]. Prepared similarly to **5**, **4** was obtained in 60% yield as yellow crystals: mp 64.5–65.5 °C (lit.[12] mp 65.5–66.5 °C); ^{1}H NMR (300 MHz, CDCl3) δ 7.36 (t, J=7.9 Hz, 1H), 7.49–7.42 (m, 2H), 7.58 (d, J=8.0 Hz, 1H), 7.94–7.84 (m, 3H), 8.77 (dd, J_1=1.6 Hz, J_2=4.8 Hz, 1H). Anal. Calcd for C_6H_4ClNO: C, 50.91; H, 2.85; N, 9.89. Found: C, 50.93; H, 2.78; N, 9.89.

*5.3.13. 2-Fluoronitrosobenzene (**5**)*[13]. To a solution of 2-fluoroaniline (0.90 mL, 9.30 mmol) in CH_2Cl_2 (20 mL), a water (80 mL) solution of Oxone® (11.0 g, 17.90 mmol) was added, and the reaction stirred at rt under N_2 atmosphere, with exclusion of light, for 24 h. The organic layer was separated and the aqueous layer was extracted with CH_2Cl_2. The combined organic layers were washed with 5% of HCl followed by satd $NaHCO_3$ and then water, dried ($NaSO_4$), and the solvents were evaporated. The residue was passed through a silica gel plug (hexane/CH_2Cl_2, 9:1) and crystallized (MeOH/H_2O) to give 460 mg (41% yield) of **5** as pale yellow crystals: mp 68–70 °C (lit.[13] mp 66–68 °C); ^{1}H NMR (300 MHz, CD_3Cl) δ 6.49 (ddd, J_1=10.5 Hz, J_2=8.5 Hz, J_3=1.8 Hz, 1H), 7.14 (t, J=7.0 Hz, 1H), 7.51 (ddd, J_1=8.0 Hz, J_2=7.0 Hz, J_3=1.1 Hz, 1H), 7.76–7.68 (m, 1H). Anal. Calcd for C_6H_4FNO: C, 57.61; H, 3.22; N, 10.94. Found: C, 56.95; H, 3.34; N, 10.94.

Acknowledgements

Financial support for this work was received from the Petroleum Research Funds (PRF-47243-AC4) and NSF (OISE 0532040).

Supplementary data

These data include 2-D NMR spectra for **1**[ClO_4], tabularized theoretical interatomic distances for **1**, distribution of spin density for **1**•, crystal data for **1a**[ClO_4] and **1d**[ClO_4], archive of calculated equilibrium geometries for **1** and **1**•, $\mathbf{1}^-$, **2**-*E*, **2**-*Z*, **1**-**TS**, **1**-**Cl**, **3**-*E*, **3**-*Z*, **3**-**TS**, **6**, and **6**-**TS**.

CCDC 792984 and 792983 contains the supplementary crystallographic data for **1a**[ClO_4] and **1d**[ClO_4]. These data can be obtained free of charge via http://www.ccdc.cam.ac.uk/conts/retrieving.html, or from the Cambridge Crystallographic Data Centre, 12 Union Road, Cambridge CB2 1EZ, UK; fax: (+44) 1223 336 033; or e-mail: deposit@ccdc.cam.ac.uk. Supplementary data associated with this article can be found in the online version, at doi:10.1016/j.tet.2011.03.023.

References and notes

1. Fozard, A.; Bradsher, C. K. *J. Org. Chem.* **1966**, *31*, 2346–2349.
2. Fozard, A.; Davies, L. S.; Bradsher, C. K.; Gross, P. M. *J. Chem. Soc. C* **1971**, 3650–3652.
3. Arai, S.; Arai, H.; Tabuchi, K.; Yamagishi, T.; Hida, M. *J. Heterocycl. Chem.* **1992**, *29*, 215–220.
4. Arai, S.; Arai, H.; Hida, M.; Yamagishi, T. *Heterocycles* **1994**, *38*, 2449–2454.
5. Norez, C.; Bilan, F.; Kitzis, A.; Mattey, Y.; Becq, F. *J. Pharmcol. Exp. Therap.* **2008**, *325*, 89–99; Roomans, G. M. *Am. J. Respir. Med.* **2003**, *2*, 413–431; Prost, A.-L.; Dérand, R.; Gros, L.; Becq, F.; Vivaudou, M. *Biochem. Pharmcol.* **2003**, *66*, 425–430; Galietta, L. J. V.; Springsteel, M. F.; Eda, M.; Niedzinski, E. J.; By, K.; Haddadin, M. J.; Kurth, M. J.; Nantz, M. H.; Verkman, A. S. *J. Biol. Chem.* **2001**, *276*, 19723–19728.
6. Wu, D.; Pisula, W.; Enkelmann, V.; Feng, X.; Müllen, K. *J. Am. Chem. Soc.* **2009**, *131*, 9620–9621.
7. Garza-Ortiz, A.; den Dulk, H.; Brouwer, J.; Kooijman, H.; Spek, A. L.; Reedijk, J. *J. Inorg. Biochem.* **2007**, *101*, 1922–1930.
8. Sinan, M.; Panda, M.; Ghosh, A.; Dhara, K.; Fanwick, P. E.; Chattopadhyay, D. J.; Goswami, S. *J. Am. Chem. Soc.* **2008**, *130*, 5185–5193.
9. Koner, R. R.; Ray, M. *Inorg. Chem.* **2008**, *47*, 9122–9124.
10. Manka, J. T.; McKenzie, V. C.; Kaszynski, P. *J. Org. Chem.* **2004**, *69*, 1967–1971.
11. Schubert, R.; Ramana, D. V.; Grützmacher, H.-F. *Chem. Ber.* **1980**, *113*, 3758–3774.
12. Campbell, N.; Henderson, A. W.; Taylor, D. *J. Chem. Soc.* **1953**, 1281–1285.
13. Darchen, A.; Peltier, D. *Bull. Soc. Chim. Fr.* **1974**, 673–676.
14. Crystal data for **1a**[ClO_4] (CCDC no. 792984): $C_{13}H_{10}ClNO_4$ triclinic, P–1, a=9.6517(12) Å, b=11.0470(13) Å, c=12.2373(15) Å, α=67.615(1)°, β=78.845(2)°, γ=87.559(2)°; V=1183.0(2) Å^3, Z=4, T=173(2) K, λ=0.71073 Å, $R(F^2)$=0.0373 or $R_w(F^2)$=0.0971 (for 4200 reflections with $I>2\sigma(I)$). Crystal data for **1d**[ClO_4] (CCDC no. 792983): $C_{12}H_9ClN_2O_4$ triclinic, P–1, a=5.9525(6) Å, b=8.3141(9) Å, c=12.2591(13) Å, α=73.487(1)°, β=83.814(1)°, γ=83.456(1)°; V=576.07(10) Å^3, Z=2, T=173(2) K, λ=0.71073 Å, $R(F^2)$=0.0414 or $R_w(F^2)$=0.1096 (for 2287 reflections with $I>2\sigma(I)$). For details see Supplementary data.
15. Smiglak, M.; Hines, C. C.; Wilson, T. B.; Singh, S.; Vincek, A. S.; Kirichenko, K.; Katritzky, A. R.; Rogers, R. D. *Chem.—Eur. J.* **2010**, *16*, 1572–1584.
16. For details see Supplementary data.
17. Wang, L.; Yi, C.; Zou, H.; Xu, J.; Xu, W. *J. Phys. Org. Chem.* **2009**, *22*, 888–896.
18. Crecca, C. R.; Roitberg, A. E. *J. Phys. Chem. A* **2006**, *110*, 8188–8203.
19. Gaenko, A. V.; Devarajan, A.; Gagliardi, L.; Lindh, R.; Orlandi, G. *Theor. Chem. Acc.* **2007**, *118*, 271–279.
20. Ammal, S. C.; Yamataka, H. *Eur. J. Org. Chem.* **2006**, 4327–4330.
21. Geibel, K.; Staudinger, B.; Grellmann, K. H.; Wendt, H. *Ber. Bunsen-Ges. Phys. Chem.* **1972**, *76*, 1246–1251.
22. Maeda, K.; Fischer, E. *Helv. Chim. Acta* **1983**, *66*, 1961–1965.
23. Brown, E. V.; Granneman, G. R. *J. Am. Chem. Soc.* **1975**, *97*, 621–627.
24. Kistiakowsky, G. B.; Smith, W. R. *J. Am. Chem. Soc.* **1934**, *56*, 638–642.
25. All reported spectra were obtained in anhydrous DMSO-d_6 taken from freshly opened ampule. Same spectra obtained in regular DMSO-d_6 with a relatively large water content show downfield shift up to 0.15 ppm for some protons.
26. Kosower, E. M. *Top. Curr. Chem.* **1983**, *112*, 117–162.
27. Becke, A. D. *J. Chem. Phys.* **1993**, *98*, 5648–5652.
28. Lee, C.; Yang, W.; Parr, R. G. *Phys. Rev. B* **1988**, *37*, 785–789.
29. Møller, C.; Plesset, M. S. *Physiol. Rev.* **1934**, *46*, 618–622; Head-Gordon, M.; Pople, J. A.; Frisch, M. J. *Chem. Phys. Lett.* **1988**, *153*, 503–506.
30. Frisch, M. J.; Trucks, G. W.; Schlegel, H. B.; Scuseria, G. E.; Robb, M. A.; Cheeseman, J. R.; Montgomery, J. A., Jr.; Vreven, T.; Kudin, K. N.; Burant, J. C.; Millam, J. M.; Iyengar, S. S.; Tomasi, J.; Barone, V.; Mennucci, B.; Cossi, M.; Scalmani, G.; Rega, N.; Petersson, G. A.; Nakatsuji, H.; Hada, M.; Ehara, M.; Toyota, K.; Fukuda, R.; Hasegawa, J.; Ishida, M.; Nakajima, T.; Honda, Y.; Kitao, O.; Nakai, H.; Klene, M.; Li, X.; Knox, J. E.; Hratchian, H. P.; Cross, J. B.; Bakken, V.; Adamo, C.; Jaramillo, J.; Gomperts, R.; Stratmann, R. E.; Yazyev, O.; Austin, A. J.; Cammi, R.; Pomelli, C.; Ochterski, J. W.; Ayala, P. Y.; Morokuma, K.; Voth, G. A.; Salvador, P.; Dannenberg, J. J.; Zakrzewski, V. G.; Dapprich, S.; Daniels, A. D.; Strain, M. C.; Farkas, O.; Malick, D. K.; Rabuck, A. D.; Raghavachari, K.; Foresman, J. B.; Ortiz, J. V.; Cui, Q.; Baboul, A. G.; Clifford, S.; Cioslowski, J.; Stefanov, B. B.; Liu, G.; Liashenko, A.; Piskorz, P.; Komaromi, I.; Martin, R. L.; Fox, D. J.; Keith, T.; Al-Laham, M. A.; Peng, C. Y.; Nanayakkara, A.; Challacombe, M.; Gill, P. M. W.; Johnson, B.; Chen, W.; Wong, M. W.; Gonzalez, C.; Pople, J. A. *Gaussian 03, Revision D.01*; Gaussian,: Wallingford CT, 2004.
31. Frisch, M. J.; Trucks, G. W.; Schlegel, H. B.; Scuseria, G. E.; Robb, M. A.; Cheeseman, J. K.; Scalmani, G.; Barone, V.; Mennucci, B.; Petersson, G. A.; Nakatsuji, H.; Caricato, M.; Li, X.; Hratchian, H. P.; Izmaylov, A. F.; Bloino, J.; Zheng, G.; Sonnenberg, J. L.; Hada, M.; Ehara, M.; Toyota, K.; Fukuda, R.; Hasegawa, J.; Ishida, M.; Nakajima, T.; Honda, Y.; Kitao, O.; Nakai, H.; Vreven, T.; Montgomery, J. A., Jr.; Peralta, J. E.; Ogliaro, F.; Bearpark, M.; Heyd, J. J.; Brothers, E.; Kudin, K. N.; Staroverov, V. N.; Kobayashi, R.; Normand, J.; Raghavachari, K.; Rendell, A.; Burant, J. C.; Iyengar, S. S.; Tomasi, J.; Cossi, M.; Rega, N.; Millam, J. M.; Klene, M.; Knox, J. E.; Cross, J. B.; Bakken, V.; Adamo, C.; Jaramillo, J.; Gomperts, R.; Stratmann, R. E.; Yazyev, O.; Austin, A. J.; Cammi, R.; Pomelli, C.; Ochterski, J. W.; Martin, R. L.; Morokuma, K.; Zakrzewski, V. G.; Voth, G. A.; Salvador, P.; Dannenberg, J. J.; Dapprich, S.; Daniels, A. D.; Farkas, O.; Foresman, J. B.; Ortiz, J. V.; Cioslowski, J.; Fox, D. J. *Gaussian 09, Revision A.02*; Gaussian,: Wallingford CT, 2009.
32. Scott, A. P.; Radom, L. *J. Phys. Chem.* **1996**, *100*, 16502–16513.

33. Stratmann, R. E.; Scuseria, G. E.; Frisch, M. J. *J. Chem. Phys.* **1998**, *109*, 8218–8224.
34. Cossi, M.; Scalmani, G.; Rega, N.; Barone, V. *J. Chem. Phys.* **2002**, *117*, 43–54 and references therein.
35. Wolinski, K.; Hinton, J. F.; Pulay, P. *J. Am. Chem. Soc.* **1990**, *112*, 8251–8260 and references therein.
36. Gottlieb, H. E.; Kotlyar, V.; Nudelman, A. *J. Org. Chem.* **1997**, *62*, 7512–7515.
37. Foresman, J. B.; Keith, T. A.; Wiberg, K. B.; Snoonian, J.; Frisch, M. J. *J. Phys. Chem.* **1996**, *100*, 16098–16104.
38. Reiss, H.; Heller, A. *J. Phys. Chem.* **1985**, *89*, 4207–4213.
39. Peng, C.; Ayala, P. Y.; Schlegel, H. B.; Frisch, M. J. *J. Comput. Chem.* **1996**, *17*, 49–56.
40. Noviandri, I.; Brown, K. N.; Fleming, D. S.; Gulyas, P. T.; Lay, P. A.; Masters, A. F.; Phillips, L. *J. Phys. Chem. B* **1999**, *103*, 6713–6722.